IEEE Access
Multidisciplinary ⋮ Rapid Review ⋮ Open Access Journal

Received September 1, 2020, accepted September 14, 2020, date of publication October 2, 2020, date of current version October 16, 2020.

Digital Object Identifier 10.1109/ACCESS.2020.3028471

Compliance Boundaries of 5G Massive MIMO Radio Base Stations: A Statistical Approach

DANIELE PINCHERA, (Senior Member, IEEE), MARCO MIGLIORE, (Senior Member, IEEE), AND FULVIO SCHETTINO, (Member, IEEE)

Department of Electrical and Information Engineering "Maurizio Scarano" (DIEI), ELEDIA, University of Cassino and Southern Lazio (UniCAS), 03043 Cassino, Italy
Inter-University Research Center on the Interactions between Electromagnetic Fields and Biosystems (ICEmB), University of Cassino and Southern Lazio, 03043 Cassino, Italy

Corresponding author: Fulvio Schettino (schettino@unicas.it)

This work was supported in part by the Ministry of Instruction, University and Research under Grant Dipartimenti di Eccellenza (2018-2022) and Grant 2017SAKZ78 [Projects of Relevant National Interest (PRIN) Multilevel methodologies to investigate Interactions between RAdiofrequencies and BIoLogIcal Systems (MIRABILIS)].

ABSTRACT In this contribution, we focus on the exposure limits and compliance distances of 5G communication systems based on large antenna arrays with high gain and multiplexing capability. In particular, starting from the observation that the antenna array continuously changes its radiation pattern to communicate with a number of user terminals, we develop a simple approach for evaluating a reliable but not overly conservative boundary for the fields radiated by the antenna array. This approach is based on the use of the Normalized Average Power Pattern, and through the paper we show its behavior and demonstrate its usefulness in some cases of interest. Finally, the obtained results are validated by means of an electromagnetic simulation of the antenna and the propagation scenario, that is achieved by means of a ray-launching code.

INDEX TERMS Antenna arrays, antenna radiation pattern, 5G systems, exposure limits, massive MIMO.

I. INTRODUCTION

5G NR [1] takes advantage of a number of technical solutions to increase bandwidth and spectral efficiency, as the extensive use of sophisticated Space Division Multiple Access (SDMA) strategies [2], in order to guarantee the unprecedented demand for data throughput. In particular, the wide use of massive Multiple Input Multiple Output (mMIMO) antennas [3], [4] allows to effectively exploit beamforming and spatial multiplexing. Beamforming allows to focus the energy transmitted by the Base Station (BS) toward a specific User Equipment (UE).

With spatial multiplexing, statistically independent information is transmitted on different spatial field configurations [5] toward a single user (Single User-Multiple Input Multiple Output, SU-MIMO) or multiple users (Multiple Users-Multiple Input Multiple Output, MU-MIMO) using the same time/frequency resources, allowing a dramatic increase of the capacity of the communication system. The counterpart of the benefits of 5G networks, is an increasing concern about the possible impact on health and safety due to exposure to radiofrequency (RF) electromagnetic radiation arising from 5G. As a matter of fact, the International Commission on Non-Ionizing Radiation Protection (ICNIRP) has given guidelines [6], which have been adopted in many countries and regions (including Europe), each with its own specific regulations, addressing the exposure limits. Such guidelines have been recently updated [7] in accordance with the latest scientific studies, and it is to be expected that national regulations will transpose them. In the following we will refer to the latest guidelines, focusing on the incident power density reference level, the application of the method to other quantities reported in the guidelines being possible.

The International Electromechanical Commission (IEC) has introduced in the standard IEC 62232:2017 [8] both measurement and computation methods for assessing compliance boundaries, both being equally valid approaches. In this regard, the use of mMIMO makes it very challenging the assessment of "realistic" compliance boundaries, as clearly explained in the IEC 62232:2017 itself: as a matter of fact, the RF EMF will vary significantly with time and in space, and the time-averaged levels relevant for RF EMF exposure assessments are significantly lower than the instantaneous peak values. In particular, the averaging period (6 minutes

The associate editor coordinating the review of this manuscript and approving it for publication was Adao Silva.

for local exposure, 30 minutes for whole body exposure [7]) is very long with respect to beamforming scheduling, resulting in a beamforming update every few milliseconds. Very different results can be obtained depending on the number and position of active users during the measurements, and assuming that all the users are at the same angle at the same time is unrealistic and leads to overestimated compliance boundaries. Consequently, stochastic approaches should be considered [8].

Even if a standard for 5G is still under development, according to the above considerations and to the standard adopted in 4G as well as previous generations, a possible candidate as EMF field level estimation procedure is based on the following two steps.

The first step is the estimation of the maximum field level in the most challenging (and indeed practically unrealistic [9]) conditions, i.e. full use of the 5G communication channel resources by a single user. This problem, know as ''maximum power extrapolation'', has recently attracted the interest of a number of research groups that have proposed some possible solutions [9]–[14].

The second step is the introduction of a reduction factor [15] to the maximum power extrapolated value that gives the EMF assessment in realistic conditions. As the technology is very recent, only a few papers address this problem. In [16], 95th percentile time-averaged output power values in a certain direction from mMIMO antennas, estimated from a mathematical model, have been reported to vary between 7% and 22% of the maximum possible output power depending upon different user distributions and exposure scenarios. In [17], the corresponding values estimated by network simulations have been reported to be 26% for Urban Macro (UMa) and 22% for Urban Micro (UMi) networks. Both models therefore confirm that the actual time-averaged RF EMF exposure is significantly lower than the theoretical maximum obtained if the BS would be transmitting at maximum power with the same beam for several minutes.

At the best knowledge of the authors, most campaigns are available for 4G networks [18], [19], which are in any case useful because LTE systems support beamforming. Only a very recently published paper considers a measurement campaign on 5G networks [20], but in all cases strong reductions are reported with respect to the conservative compliance value due to beamforming.

This paper is focused on the statistical analysis of the 5G EMF level in a number of realistic conditions considering the main architectures of radiating systems involved in 5G, i.e. beamforming arrays and MU-MIMO antennas.

Section II introduces the Normalized Average Power Pattern (NAPP) as a tool to estimate the reduction factor due to the stochastic processes underlying the communication process. In Section III the NAPP is applied to phased array antennas. In particular, a statistical estimation of the NAPP at the 95 quantile (Q-NAPP) is considered, showing that it is possible to obtain a simple and intuitive representation of the reduction factor in the whole space around the antenna.

Section IV is devoted to the analysis of the role of the main design parameters of the antenna (number of elements, element pattern) as well as of the geometry of the area served by the communication systems (e.g. angular dimension of the served area, geometry of the cell) on Q-NAPP.

Section V discusses the important problem of the EMF estimation in case of MU-MIMO communications. The analysis of the EMF level in a number of realistic conditions depends on the details of the scheduler of the communication network, that is not standardized. In this paper, we use a modified version of the zero-forcing algorithm, that showed good stability properties. For sake of reader convenience, the modified zero-forcing algorithm is described in the Appendix, while for an electromagnetic analysis of MU-MIMO communication systems the interested reader is invited to refer to [21], [22].

The method is used in Section VI to estimate the compliance distances in the cases previously analyzed, whereas Section VII extends the Q-NAPP estimation to a more sophisticated model, based on ray-tracing.

Finally, conclusions are discussed in Section VIII.

The results reported in this paper give a general picture of the reduction level of the EMF in realistic conditions and confirm the significant reduction of the average field level associated to the use of modern 5G antennas.

II. NORMALIZED AVERAGE POWER PATTERN

In this section we will introduce and discuss the concept of Normalized Average Power Pattern, a tool that will be used to analyse the exposure limits in 5G communication systems.

Let us now consider a BS antenna array in free space, centred in the origin of a spherical coordinate system (ρ, θ, ϕ), that is transmitting a certain power P_T to a single user that is in a specific angular position (θ_1, ϕ_1). The power density radiated by the antenna $S_1(\rho, \theta, \phi)$ is well approximated in the ''far field'' of the array by:

$$S_1(\rho, \theta, \phi) = \frac{P_T}{4\pi\rho^2} G_1(\theta, \phi) \tag{1}$$

where $G_1(\theta, \phi)$ is the array gain when its excitation has been configured for communicating with the aforementioned single user.

Once the power density is calculated, the compliance boundary in this case can be evaluated according to:

$$S(\rho, \theta, \phi) \leq S_M \tag{2}$$

where S_M is the maximum acceptable power density [7].

In 5G communication systems we usually have many different users, and the compliance boundary in (2) needs to be calculated on an average radiation occurring in a time T_A, that is 6 minutes for local body exposure and 30 minutes for whole body exposure [7].

In the hypothesis that only a single user, among K possible users, is served by the BS at the same time (such an hypothesis will be later removed), and the maximum power is transmitted

toward such a user, we could calculate the average radiated power density as:

$$\begin{aligned} S_A(\rho,\theta,\phi) &= \frac{P_T}{4\pi\rho^2}\frac{1}{T_A}\sum_{k=1}^{K} G_k(\theta,\phi)T_k \\ &= \frac{P_T}{4\pi\rho^2}\sum_{k=1}^{K} G_k(\theta,\phi)\tau_k \\ &= \frac{P_T G_M}{4\pi\rho^2}\sum_{k=1}^{K}\frac{G_k(\theta,\phi)}{G_M}\tau_k \\ &= \frac{P_T G_M}{4\pi\rho^2}\mathcal{N}_K(\theta,\phi) \end{aligned} \tag{3}$$

where G_k is the gain when the antenna is configured to radiate towards the k-th user, G_M is the maximum array gain, and T_k is the time allocated for the k-th user, so that $\sum_{k=1}^{K} T_k = T_A$ if the array is used in downlink for 100% of the time, and $\tau_k = T_k/T_A$ represents the fraction of time allocated for the k-th user, and $\mathcal{N}_K(\theta,\phi)$ is the Normalized Average Power Pattern (NAPP):

$$\mathcal{N}_K(\theta,\phi) = \sum_{k=1}^{K}\frac{G_k(\theta,\phi)}{G_M}\tau_k \tag{4}$$

where the subscript K is used to remember that the NAPP depends on the particular choice of the K random directions considered in the average.

The NAPP represents the average fraction of power radiated in a certain direction, with respect to the maximum possible power. A value of NAPP of 0.1 in a specific direction means that during the T_A the BS array would radiate in that direction only a tenth of the power it would radiate when focusing its beam using the maximum gain 100% of the time. This quantity is similar to the parameter G_{avg}, introduced in [20], which is an average gain, obtained "experimentally", by means of the analysis of the information collected by the 5G BSs operation for 24 h over a weekday.

The analysis of the NAPP could allow the determination of the shape of the compliance boundary:

$$\mathcal{R}(\theta,\phi) \geq R_M(\theta,\phi) = \sqrt{\frac{P_T G_M}{4\pi S_M}\mathcal{N}_K(\theta,\phi)} \tag{5}$$

where $\mathcal{R}(\theta,\phi)$ gives the radial coordinate with respect to the centre of the antenna where the exposure limits are satisfied, and $R_M(\theta,\phi)$ gives the radial coordinate of the surface within which the exposure limits are not satisfied: such a boundary would depend upon the number of users, their connection times, their movement and so on; this means that a deterministic analysis is not possible, and this problem needs to be faced by a statistical approach.

III. A STATISTICAL APPROACH

In this section we will analyse, by means of a statistical approach, the behaviour of the NAPP function. To accomplish this task we need to choose a reasonable scenario for our simulations.

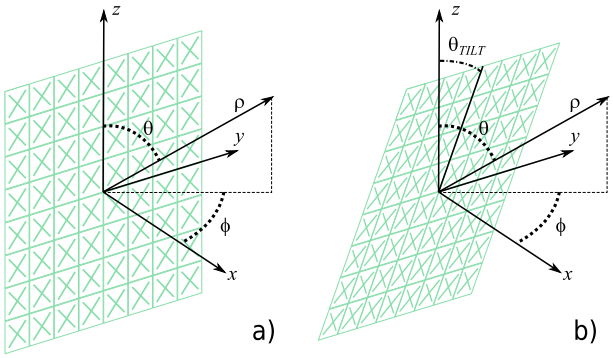

FIGURE 1. Scheme of the 8 × 8 antenna array and of the coordinate systems employed: a) the array elements are in the yz plane; b) the array plane is rotated of an angle θ_{TILT} around $y-$axis.

As a preliminary analysis, we start considering an 8 × 8 planar array of $\lambda/2$ equispaced elements (see Fig. 1a); this kind of array is similar to the arrays currently used for 5G communication systems, to offer a coverage of 120° (deg) on the azimuthal plane, and 30° (deg) on the vertical plane.

Now, according to what has been discussed in the previous Section, we are going to analyse the NAPP in some working scenarios; for the sake of simplicity in each scenario we are going to suppose that $\tau_k = T_K/T_A = 1/K$, i.e. the users have a uniform allocation in time and the BS antenna is working "full load".

In the first one we will consider that the users directions (θ_k, ϕ_k) are uniformly distributed in the 30° × 120° angular region, and the antenna elements are simple isotropic elements. If we suppose that $K = 200$, we can calculate the NAPP using for $G_k(\theta,\phi)$ the gain of the antenna array when the amplitude of the elements' excitation is uniform and a linear phase shift is used in order to obtain a beam focused in the direction (θ_k, ϕ_k). The result of the NAPP calculation for one specific realization of users distribution is given in Fig. 2 as an example. It is clearly visible that the NAPP presents a non uniform behaviour, due to the randomness of angular position of the terminals: each different set of users would result in a different NAPP.

In order to correctly characterize the compliance distance we need to face this problem by means of a statistical approach. To this task, we analysed $N = 10000$ different sets of random users, with an angular position (θ_k, ϕ_k) uniformly distributed in the 30° × 120° angular region.

The mean NAPP of these random sets can be calculated and is depicted in Fig. 3. This plot gives us an idea of what is the mean power distribution around the antenna (this plot is much more regular than the previous), but does not help us very much in building a safe compliance boundary.

In Fig. 4 we show the cumulative density function (CDF) for the NAPP, for some relevant directions. A better approach consists in evaluating, for each direction (θ,ϕ) the quantiles of the distribution of the normalized average power pattern (Q-NAPP).

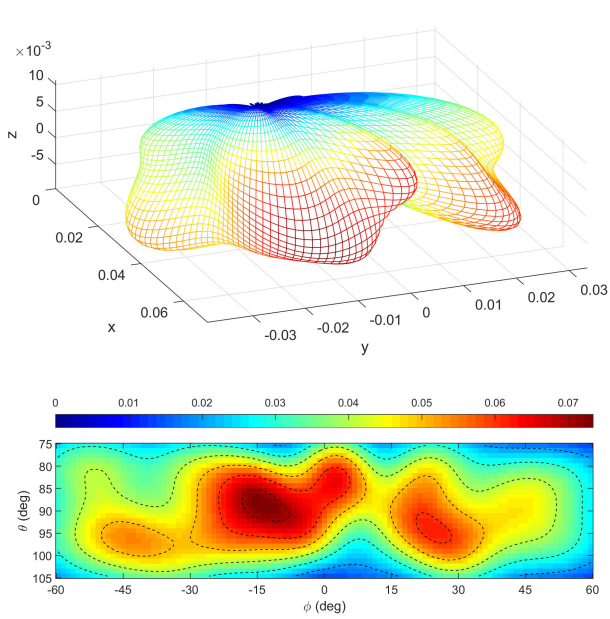

FIGURE 2. The NAPP function for a set of $K = 200$ random directions. Upper plot: 3D representation of the function. Lower plot: imagemap of the function, restricted to the scanning region. The contour curves are calculated for the values of the "ticks" of the colorbar.

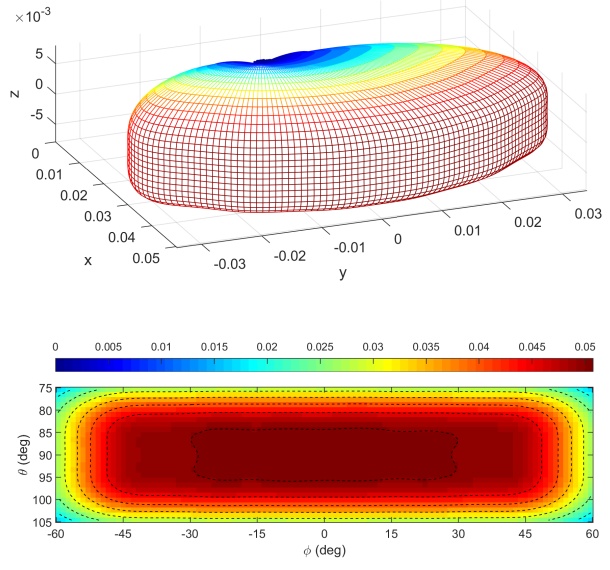

FIGURE 3. The mean NAPP function, calculated on 10000 random sets of $K = 200$ random directions. Upper plot: 3D representation of the function. Lower plot: imagemap of the function, restricted to the scanning region. The contour curves are calculated for the values of the "ticks" of the colorbar.

In Fig. 5 it is possible to see the 95% quantile $\mathcal{N}_{q=0.95}(\theta, \phi)$; the peak value of this distribution is 0.0690, while the mean value[1] is 0.0569. As a matter of fact, the peak value of the Q-NAPP is exactly equivalent to the power

[1]Calculated in the 30° × 120° angular region

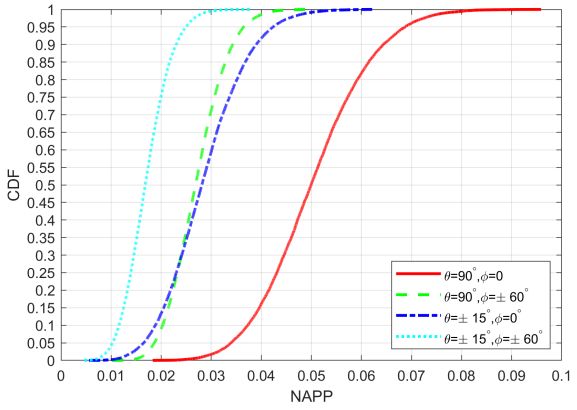

FIGURE 4. Cumulative density function (CDF) for the NAPP calculated for some relevant directions.

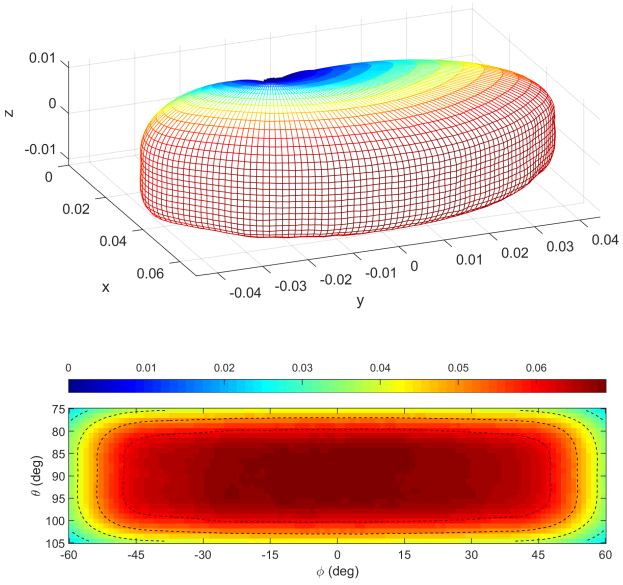

FIGURE 5. The 95% quantile of NAPP function, calculated on 10000 random sets of $K = 200$ random directions. Upper plot: 3D representation of the function. Lower plot: imagemap of the function, restricted to the scanning region. The contour curves are calculated for the values of the "ticks" of the colorbar.

reduction factor (F_{PR}) used in [15], and the two terms will be used indifferently in the following.

Now we could use this function to calculate the distance from the source that guarantees for each direction the satisfaction of the exposure limits in 95% of the cases:

$$\mathcal{R}_{q=0.95}(\theta, \phi) = \sqrt{\frac{P_T G_M F_{TDD}}{4\pi S_M} \mathcal{N}_{q=0.95}(\theta, \phi)} \qquad (6)$$

where F_{TDD} is a value in the range (0, 1) modeling the fact that in the Time Domain Duplex (TDD), the antenna transmits only for a fraction of time.

As an example, in Fig. 6 we provide the calculation of the boundary of the exclusion zone, i.e. the boundary of the region in which the exposure limits are not verified, for a

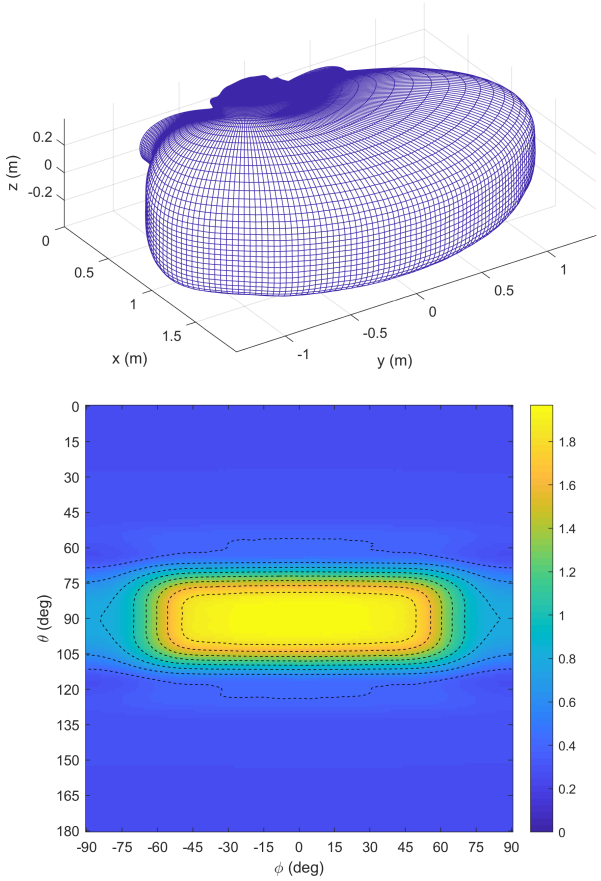

FIGURE 6. The exclusion zone calculated from the 95% quantile of NAPP function. Upper plot: 3D representation of the boundary of the exclusion zone. Lower plot: imagemap of the $R_{q=0.95}$ function. The contour curves are calculated for the values of the "ticks" of the colorbar.

transmitted power $P_T = 50$W, an exposure limit $S_M = 10\text{W/m}^2$, and $F_{TDD} = 0.75$; for the value of G_M we have employed the value of 22.75dB, since we have supposed to use isotropic elements radiating only in one half-space with respect to the plane of the array. The maximum value of $R_{q=0.95}(\theta, \phi)$ is $1.97m$.

Obviously, other quantiles like 0.9 or 0.99, could be taken into account; for the sake of simplicity in this paper we will always consider the 0.95 quantile.

IV. INFLUENCE OF THE SYSTEM PARAMETERS ON THE Q-NAPP

First of all, in the previous simulation we have considered a set of $K = 200$ random angular positions of users to calculate the NAPP. Such a value has been estimated considering that the network is working "full load", with an average transfer rate per user of 5Mbps (corresponding to the streaming of a full-hd compressed video or the download of about 200MB of data, a medium size mobile APP, during $T_A = 6$ min), and a BS throughput of 1Gbps. A smaller number of users loading the network in the same way would imply a value of $\tau_k < 1/K$, and hence a smaller value of the NAPP.

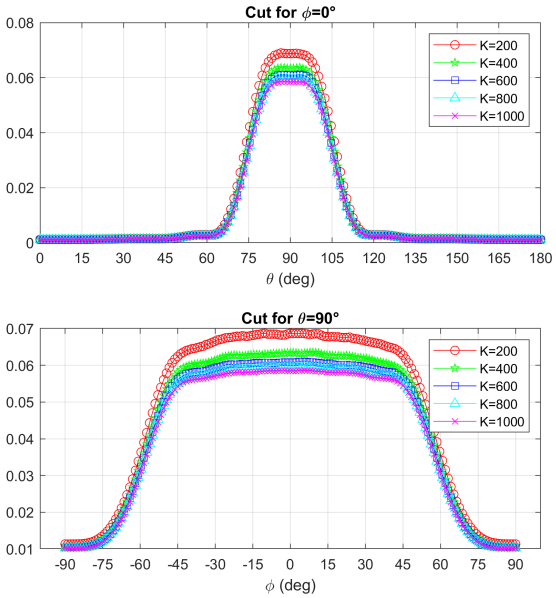

FIGURE 7. Relevant cuts of the Q-NAPP function for some values of K.

TABLE 1. The values of the peak and average of the Q-NAPP for some values of K.

Case	mean $\mathcal{N}_{q=0.95}$	peak $\mathcal{N}_{q=0.95}$
$K = 200$	0.0569	0.0690
$K = 400$	0.0524	0.0636
$K = 600$	0.0504	0.0612
$K = 800$	0.0492	0.0598
$K = 1000$	0.0484	0.0587

In Fig.7 we compare the main cuts of Q-NAPP for some values of K; as it is clearly seen, all the resulting curves are very close, and $K = 200$ represents a sort of "worst case". Such a value will be kept for the successive calculations in the next paragraphs. The obtained values of the peak and average of the Q-NAPP are provided in table 1.

It is worth stressing that, considering the same working scenario, lower values of K correspond to higher values of the NAPP, since when the number of users is very high, the field distribution around the BS antenna, resulting from the averages of the pattern radiated in all the users' directions, would be very smooth. When the users' number becomes smaller, there are chances that in some directions there could be a cluster of users would be higher, thus resulting in a higher peak of the NAPP.

It may be possible to use lower values of K in the analysis, but according to the discussion at the beginning of this section, a smaller number of K would lead to a network that is not fully loaded; similar considerations are also reported in the discussion section of [20].

A. ELEMENT PATTERN

The previous results were obtained with an isotropic element pattern; if we use a $\sin(\theta)$ element pattern, typical of a short dipole antenna, we would obtain results very close to the

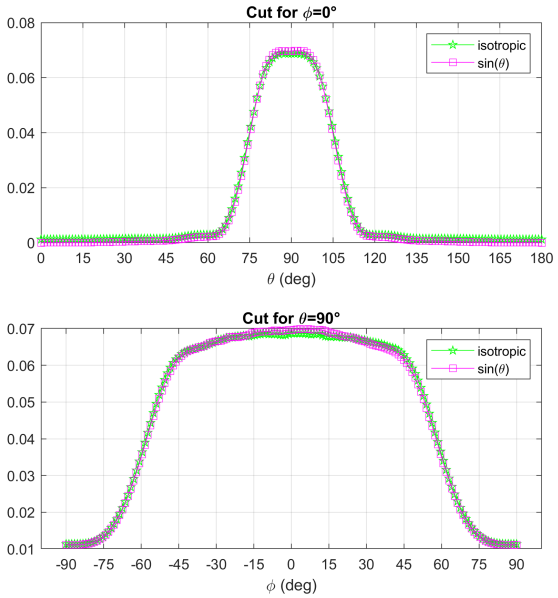

FIGURE 8. Relevant cuts of the Q-NAPP function when the element pattern is modified.

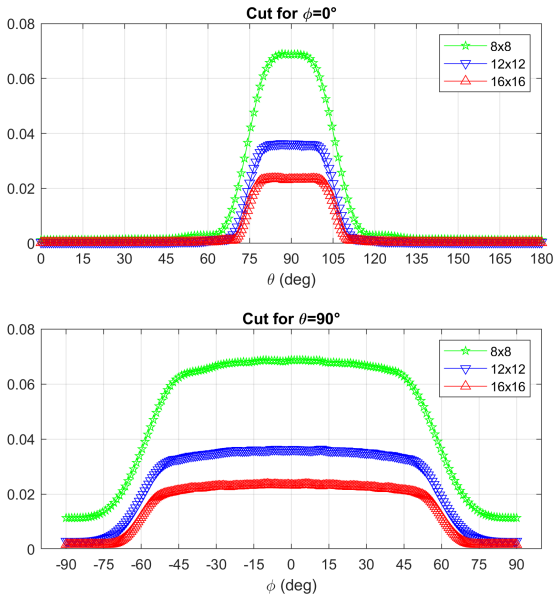

FIGURE 9. Relevant cuts of the Q-NAPP function when the number of elements is modified.

previous ones (see Fig. 8): the mean of the Q-NAPP increases from 0.0569 to 0.0594 and the peak increases from 0.0690 to 0.0701. The reason is two-fold: first, the element pattern does not significantly change in the focusing region; second, using this element pattern the directivity of the broadside beam of the antenna is increased from 19.74dB to 19.97dB: a small variation due to the fact that the greatest contribution for the directivity comes from the array factor and not from the element factor.

Generally speaking, if the element pattern is well designed, i.e. does not change significantly in the focusing region, not to reduce too much the directivity of the beam, its influence on the NAPP will be limited. For this reason, unless differently stated, we will use a simple isotropic pattern in the following.

B. NUMBER OF RADIATING ELEMENTS

A second aspect to be investigated is the influence of the number of array elements. For 5G systems, it is not particularly significant the case of a smaller number of elements, so we have considered two different array dimensions 12×12 and 16×16.

As it is clearly visible from Fig. 9 the increase of the number of elements has a strong impact on the NAPP; in particular, the beam-width of the focused beam will be smaller, and this will result in a smaller probability that more beams, focused in close directions sum up and increase the peak value of the NAPP.

The values of the Q-NAPP become much smaller with the increase of the number of elements (see also the values given in table 2), but we have to remember that also the array gain would increase significantly, and the compliance boundary of (5) may see a slight increase because of the multiplication of the two factors G_M and $\mathcal{N}_{q=0.95}$ (see Table 6).

TABLE 2. The values of the peak and average of the Q-NAPP when the number of elements is modified.

Case	mean $\mathcal{N}_{q=0.95}$	peak $\mathcal{N}_{q=0.95}$	G_M (dB)
8×8	0.0569	0.0690	19.74
12×12	0.0315	0.0365	23.34
16×16	0.0207	0.0237	25.89

TABLE 3. The values of the peak and average of the Q-NAPP when the scanning region is modified.

Case	mean $\mathcal{N}_{q=0.95}$	peak $\mathcal{N}_{q=0.95}$
$30° \times 120°$	0.0569	0.0690
$45° \times 120°$	0.0428	0.0507
$60° \times 120°$	0.0355	0.0410
$30° \times 90°$	0.0727	0.0878
$30° \times 60°$	0.1020	0.1228

C. SCANNING REGION

The specification of the size of the scanning region ($30° \times 120°$) was inspired by the suggested scanning region for some commercially available 5G antennas; in this case such a shape is intended for the use in a 120° sectoral coverage.

We have also tested the effect of considering different shapes for the scanning region, and in particular we have tested ($45° \times 120°$), ($60° \times 120°$), ($30° \times 90°$) and ($30° \times 60°$); the results are given in fig. 10 and table 3. As it is intuitive, increasing the size of the scanning region results in a decrease of the NAPP, whereas a decrease of the scanning region would result in an increase of the NAPP.

D. SWITCHED BEAMS

In many commercially available antenna systems the focusing towards the terminals is achieved by a "grid of beams",

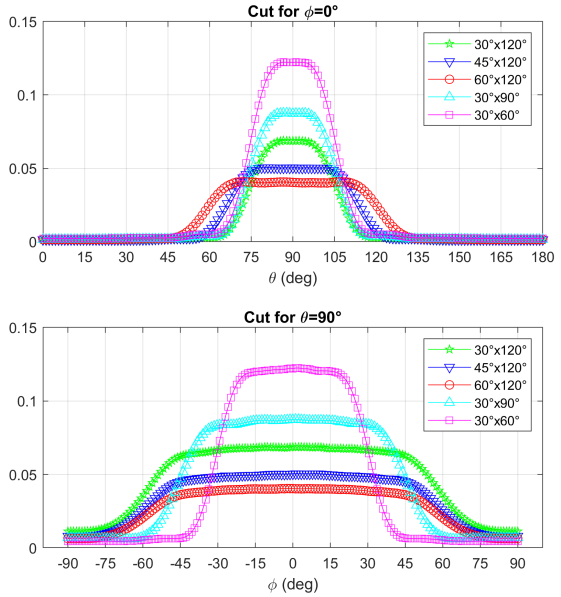

FIGURE 10. Relevant cuts of the Q-NAPP function when the scanning region is modified.

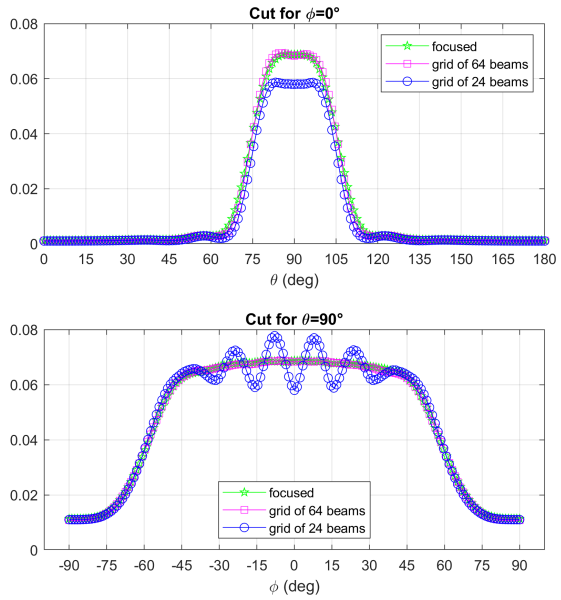

FIGURE 11. Relevant cuts of the Q-NAPP function when the grid of beams is employed.

so the antenna can be configured to radiate some specific beams. To test the effect of the grid of beams on the NAPP, we have considered two grids: the first grid of 64 beams (16 directions on ϕ and 4 directions on θ), the second of 24 beams (8 directions on ϕ and 3 directions on θ), to cover the (30° × 120°) sector. Each user is then served by the beam allowing the maximum received power selected from the grid. The result of the first grid is very close to the case in which the beam is freely focusable in the region; in the case of the second grid we instead see a significant ripple of the Q-NAPP, due to the envelope of the beams (see Fig.11 and table 4).

TABLE 4. The values of the peak and average of the Q-NAPP when the grid of beams is employed.

Case	mean $\mathcal{N}_{q=0.95}$	peak $\mathcal{N}_{q=0.95}$
free focusing	0.0569	0.0690
grid of 64 beams	0.0594	0.0696
grid of 24 beams	0.0582	0.0779

E. TERMINALS ON PLANE REGION

The choice of considering terminals uniformly distributed in the (θ, ϕ) directions allows to get a preliminary insight on the behaviour of the considered antenna system. However, it is of interest to investigate different and more realistic distributions [18]. In our paper we will consider the elements uniformly placed on a planar area, with the shape of an angular sector or the shape of an hexagon, and we will calculate the actual angle of arrival of the signals towards the position of the users.

An example of the angular distributions, resulting from the uniformly random placement of the terminals in the cell, for a BS at an height of 30m above the planar area, is given in Fig.12. It must be underlined that the angles of the signal are represented with respect to the spherical coordinate system with the vertical axis orthogonal to the horizontal plane where the terminals are placed (see Fig. 1).

The antenna array will be tilted of an angle $\theta_{TILT} = 20.13°$ (deg) as in Fig.1b, in order to mimic the $(30° \times 120°)$ coverage for users having a distance from the array in the range $d_{min} \leq d \leq d_{max}$ with $d_{min} = 42.6m$ and $d_{max} = 333.5m$. It has to be noted that there could be users at closer positions with respect to the antenna array, but since the distribution of the users is uniform on the plane, the presence of elements with $d \leq d_{min}$ would not change the Q-NAPP significantly. In all the simulations dealing with users distributed on the plane the antenna tilting has been taken into account.

As it is clearly visible from Fig.13 and Fig.14, the Q-NAPP shows a much different behavior with respect to the previous cases, with much "thinner" distributions, with an higher peak value (0.1231 for the sectoral cell, and 0.1734 for the hexagonal cell). As it will be shown in section VI, such a strong variation of the peak will have a smaller impact on the size of the compliance distance.

V. MULTIPLE LAYERS

In the previous section we have considered the hypothesis that the antenna array communicates with a single terminal at a time, using all its power to focus the beam towards the desired user. In this way the time/domain resources are divided among the users, while beamforming allows to increase the SNR at the receiver.

A more sophisticated SDMA technique is based on the use of different spatial field configurations to transmit independent information exploiting multiple parallel channels that share the same time/frequency resource [21]. Two different approaches are available: multiple data streams can be sent to a single user (SU-MIMO) or to multiple users (MU-MIMO).

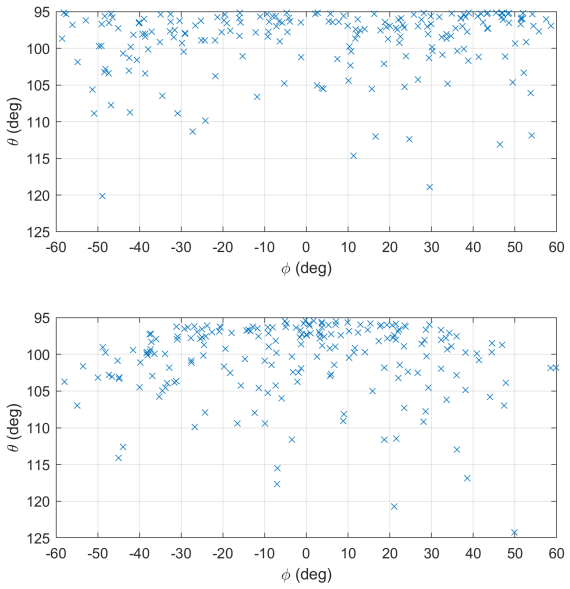

FIGURE 12. Example of the resulting angular distribution of the signals with respect to the array for $K = 200$. Upper subplot: sectoral cell. Lower subplot: hexagonal cell.

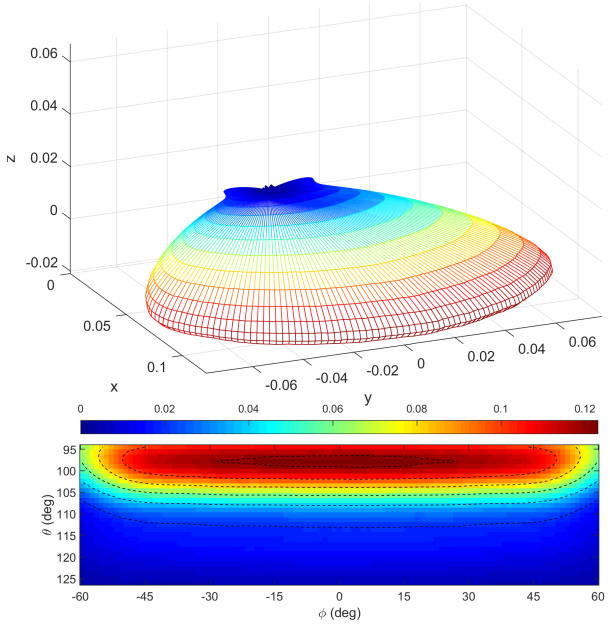

FIGURE 13. The 95% quantile of NAPP function, calculated on 10000 random sets of $K = 200$ random directions on the sectoral cell. Upper plot: 3D representation of the function. Lower plot: imagemap of the function, restricted to the scanning region. The contour curves are calculated for the values of the "ticks" of the colorbar.

These techniques represent a sophisticated solution for the reuse of the highly precious time/frequency resources made available by the communication channels: the data stream is divided into sub streams, associated to different communication "layers". Current 5G communication systems allow up to 16 layers associated up to 8 different users [9].

For the sake of simplicity, in this paper we will analyze only the MU-MIMO case, with a single layer associated to each user. In order to analyze the impact of the use of multiple

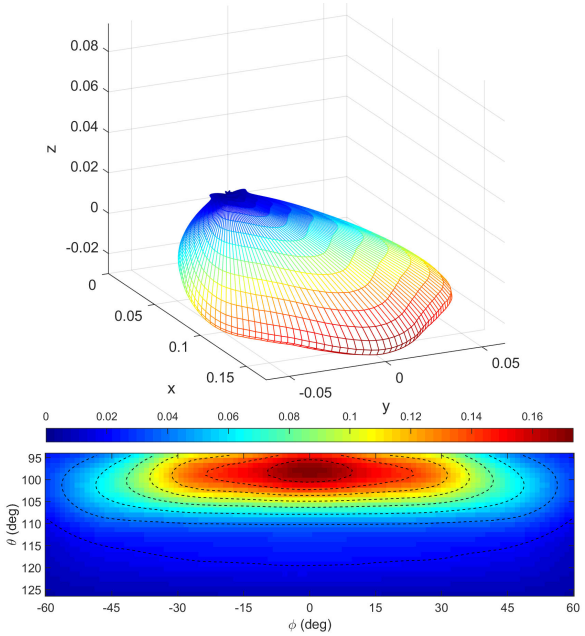

FIGURE 14. The 95% quantile of NAPP function, calculated on 10000 random sets of $K = 200$ random directions on the hexagonal cell. Upper plot: 3D representation of the function. Lower plot: imagemap of the function, restricted to the scanning region. The contour curves are calculated for the values of the "ticks" of the colorbar.

layers, let us suppose that the antenna uses a fixed number of layers L, for the entire duration of the T_A; i.e., the array communicates with a number L of terminals at the same time. This communication will be realized using a zero-forcing approach, that has been demonstrated to be very close to the optimal approach [23], [24].

When communicating with the L terminals, the transmitted power will be equally split among the L terminals, but each terminal would have been allocated for a time $\tau_k = L/K$: the calculation of the NAPP could be performed using (4), provided that the pattern gains are calculated taking into account that in the zero forcing we require the pattern of the beam used to communicate with a terminal, to have a null towards the direction of the other $L - 1$ terminals.

The simulation has been performed in this way: for each of the N scenarios, a set K=200 directions is randomly generated. Then the users are grouped into sets of L terminals using the scheduling algorithm described in the Appendix. For each group of L terminals the excitation coefficients of the array elements that realize the zero-forcing are calculated, and from those coefficients we obtain the array gains to use in (4).

As it is possible to see from Fig.15, up to 4 layers, the values of the Q-NAPP are very close to the values of the single layer case. This behaviour is also confirmed in other working scenarios; just as an example in Fig.16 and Fig.17, when the distribution of terminals is uniform on the sectoral cell or on hexagonal cell.

The reason of this behavior is the reduction of the gain when using a zero forcing approach, with respect to the case of a "free" focusing towards the terminals. When we impose a number of zeros in the un-wanted directions, we are using

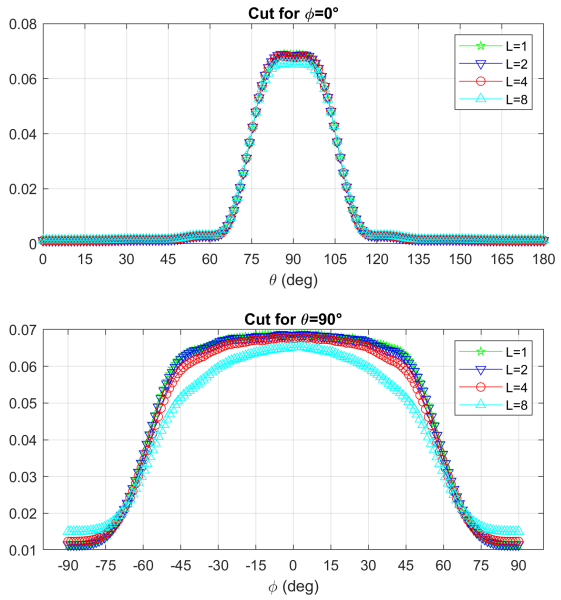

FIGURE 15. Relevant cuts of the Q-NAPP function when multiple layers are employed: uniform random distribution of terminals on 30° × 120° angular region.

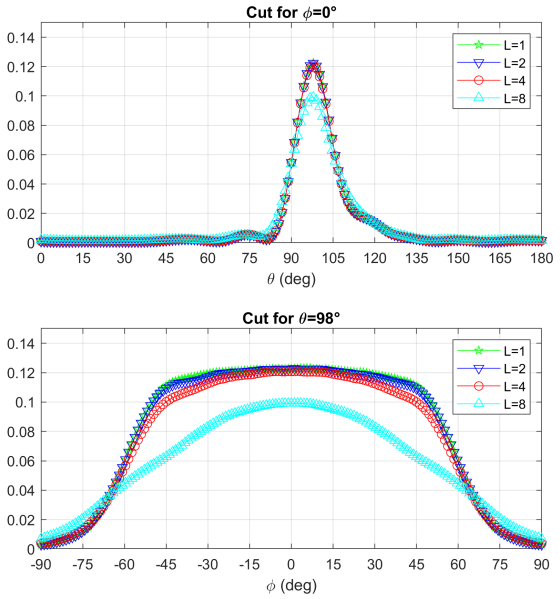

FIGURE 16. Relevant cuts of the Q-NAPP function when multiple layers are employed: uniform distribution of terminals on sectoral cell.

TABLE 5. The values of the peak and average of the Q-NAPP when multiple layers are employed.

Case	mean $\mathcal{N}_{q=0.95}$	peak $\mathcal{N}_{q=0.95}$
scan 30° × 120° — $L = 1$	0.0569	0.0690
scan 30° × 120° — $L = 2$	0.0567	0.0690
scan 30° × 120° — $L = 4$	0.0559	0.0684
scan 30° × 120° — $L = 8$	0.0522	0.0655
sector 120° — $L = 1$	0.0522	0.1231
sector 120° — $L = 2$	0.0519	0.1228
sector 120° — $L = 4$	0.0505	0.1210
sector 120° — $L = 8$	0.0424	0.0992
hexagon 120° — $L = 1$	0.0505	0.1734
hexagon 120° — $L = 2$	0.0501	0.1695
hexagon 120° — $L = 4$	0.0485	0.1516
hexagon 120° — $L = 8$	0.0419	0.0889

some of the degrees of freedom of our array, and this would result in a slight reduction of the peak gain with respect to the unconstrained case.

It must be underlined the analyzed trend is due to the use of a specific antenna array and channel model considered, as well as the signal processing chosen, that tries to impose zeroes of the field in some specific directions. A modification, for instance, of the antenna array geometry or of the signal processing performed may lead to different results but - in any case - the NAPP will show a non-increasing behavior with a increasing value of L: the single layer case represents the worst case for the analysis of the NAPP.

VI. COMPLIANCE DISTANCE AND POWER REDUCTION FACTOR

In this section we provide the calculation of the compliance distances and power reduction factors for the previously considered cases. The cases are listed in Table 6, were we provide

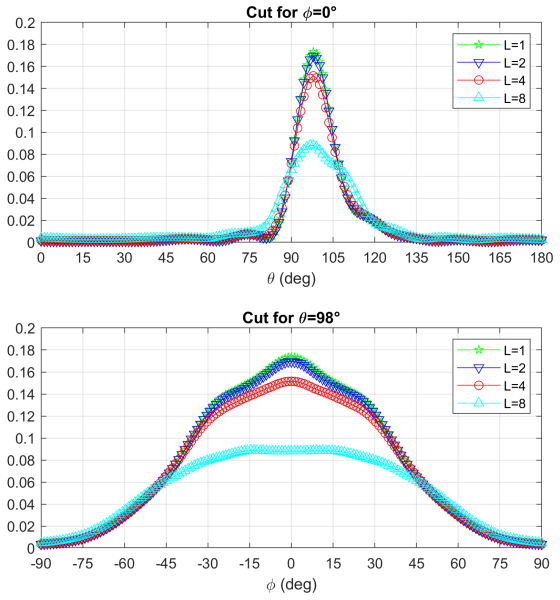

FIGURE 17. Relevant cuts of the Q-NAPP function when multiple layers are employed: uniform distribution of terminals on hexagonal cell.

the maximum value of $R_{q=0.95}(\theta, \phi)$ and the value of the power reduction factor F_{PR} [15], evaluated as:

$$F_{PR} = \max_{\theta,\phi} \mathcal{N}_{q=0.95}(\theta, \phi). \tag{7}$$

For the calculations we have used a transmitted power $P_T = 50\text{W}$, an exposure limit $S_M = 10\text{W}/m^2$, and $F_{TDD} = 0.75$; for the value of G_M we have employed the value of 22.75dB, 26.35dB and 28.90dB, for the 8 × 8, 12 × 12 and 16 × 16 respectively, since we have supposed to use isotropic

TABLE 6. Data for the compliance distances and power reduction factors for the considered cases.

Case	max $R_q(\theta,\phi)$	F_{PR}
8×8 — scan $30°\times120°$ — $L=1$	$1.97m$	0.0690
12×12 — scan $30°\times120°$ — $L=1$	$2.17m$	0.0365
16×16 — scan $30°\times120°$ — $L=1$	$2.34m$	0.0237
8×8 — scan $45°\times120°$ — $L=1$	$1.69m$	0.0507
8×8 — scan $60°\times120°$ — $L=1$	$1.52m$	0.0410
8×8 — scan $30°\times90°$ — $L=1$	$2.22m$	0.0878
8×8 — scan $60°\times60°$ — $L=1$	$2.63m$	0.1228
8×8 — "grid of beams" 64 — $L=1$	$1.97m$	0.0696
8×8 — "grid of beams" 24 — $L=1$	$2.09m$	0.0779
8×8 — scan $30°\times120°$ — $L=2$	$1.97m$	0.0690
8×8 — scan $30°\times120°$ — $L=4$	$1.96m$	0.0684
8×8 — scan $30°\times120°$ — $L=8$	$1.92m$	0.0655
8×8 — sector $120°$ — $L=1$	$2.62m$	0.1231
8×8 — sector $120°$ — $L=2$	$2.63m$	0.1228
8×8 — sector $120°$ — $L=4$	$2.61m$	0.1210
8×8 — sector $120°$ — $L=8$	$2.36m$	0.0992
8×8 — hexagon $120°$ — $L=1$	$3.12m$	0.1734
8×8 — hexagon $120°$ — $L=2$	$3.09m$	0.1695
8×8 — hexagon $120°$ — $L=4$	$2.92m$	0.1516
8×8 — hexagon $120°$ — $L=8$	$2.23m$	0.0889

elements radiating only in one half-space with respect to the plane of the array.

Just as a reference, we have calculated the values of maximum $R_M(\theta,\phi)$ that we would have when considering a fixed beam pattern pointing in the same direction for the whole T_A: for the 8×8 array we obtain $7.49m$, for the 12×12 array we obtain $11.35m$, for for the 16×16 array we obtain $15.21m$. The greater the array gain, the more overly conservative become the distances for the exposure limits without a proper statistical characterization of the array. On the other hand, the reduction factor estimated with the proposed method for the 8×8 array covering a $30°\times120°$ scanning region, ranging between 6.5% and 17.3% in the cases reported in Table 6, are in perfect agreement with values evaluated in [16], [17], [20].

It is important to underline that the distances provided in Table 6 have been evaluated considering a far-field approximation, and if we consider a typical operation frequency for arrays of that kind, $f_0 = 3.7GHz$, we find a far field distance ($r = 2d^2/\lambda$) of about 4 meters for the 8×8 array, about 10 meters for the 12×12 array and about 18 meters for the 16×16 array. Since we are not in the reactive-field region of the array, by means of numerical simulations (not provided here for the sake of brevity) we have verified that only the nulls and the lowest lobes of the patterns are modified at the distances of interest, so the results provided represent a very good approximation, that should be verified in the specific case by means of in-situ measurements.

VII. EVALUATION OF NAPP IN RAY-TRACING MODELED URBAN SCENARIOS

The above analysis was carried out in free-space. However, NAPP is a very flexible tool that can be applied also in more complex and realistic scenarios.

A widely adopted approach to study the propagation in urban area is based on ray tracing simulation [25].

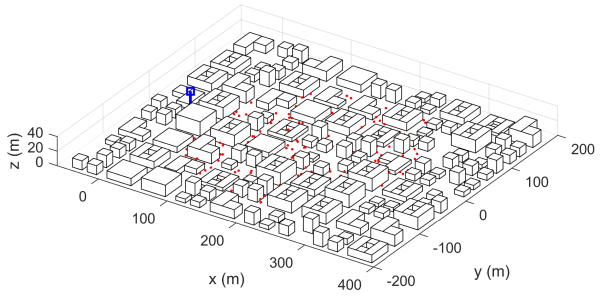

FIGURE 18. The model of the city considered for the ray-launching analysis and with an example of the positions of the terminals (red dots) and the position of the BS array (blue square).

Consequently, it is of interest to integrate the NAPP approach in ray-tracing code.

In this Section we will show an example of the use of NAPP in a ray-tracing simulation. The results reported in the Section will show not only the effectiveness of the integration of the NAPP approach in the ray-tracing code considering urban scenarios illuminated by realistic double-polarized antenna arrays, but will also show that the results are quite close to the ones obtained in the previous analyzed free-space conditions, thus validating the proposed method as a practical and truthful solution to compute compliance boundaries.

In particular, the antenna array will be modelled as a 8×8 grid of dual polarized elements ($\pm45°$ linearly polarized short wires), at a height of 30m over the ground, and the terminals will be placed at a height of 1.5m over the ground in a test city (see Fig. 18), that is simulated by means of a custom ray-tracing algorithm coded in Matlab, using the ray-launching (or pincushion) method with up to 20 reflections (this is a conservative upper bound, as much less reflections are usually needed). The reflections of the rays on the surfaces (ground or buildings) are calculated according to the proper TE or TM coefficients (or a proper combination of them) according to the polarization of the incoming ray. The relative permittivity of the materials is chosen equal to 4, a value that correctly simulates the electromagnetic behaviour of typical grounds and concrete.

The city is procedurally generated, with square blocks of flats of 50m side, street width of 15m meters, variable shape of the buildings in the square block and variable height of the building between 4m and 20m.

In this scenario the users are uniformly distributed on the ground, in a hexagonal cell of 333m diameter; there are no users inside the buildings or outside the considered hexagonal cell.

The graph of the Q-NAPP, calculated averaging over 1000 different scenarios for the case of a single layer and 200 users positions, is provided in Fig.19. This plot is very similar to the plot of Fig.14, but it is slightly unsymmetrical, because of the lack of symmetry in the model of the city used for the electromagnetic simulation.

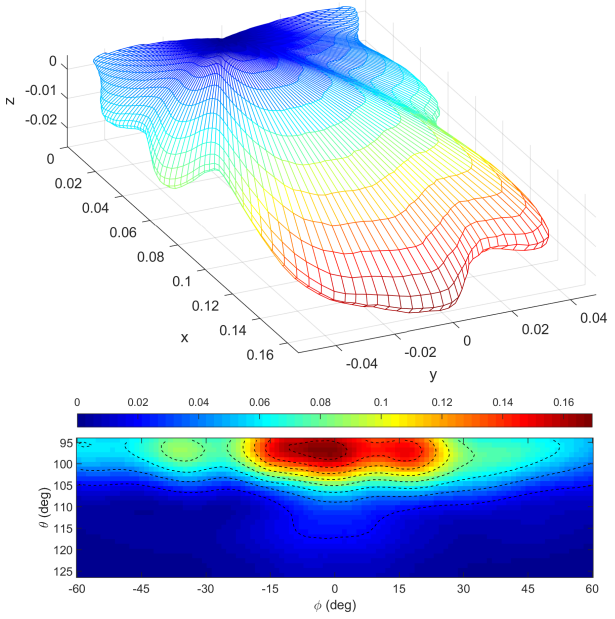

FIGURE 19. The 95% quantile of NAPP function, calculated on 1000 random sets of $K = 200$ random users in the city with $L = 1$. Upper plot: 3D representation of the function. Lower plot: imagemap of the function, restricted to the scanning region. The contour curves are calculated for the values of the "ticks" of the colorbar.

TABLE 7. Data for the compliance distances and power reduction factors when the users are in the simulated city.

Layers	max $R_q(\theta, \phi)$ (m)	F_{PR}
1	3.17	0.1694
2	3.17	0.1694
4	3.00	0.1520
8	2.28	0.0874

The Q-NAPP analysis has been also repeated with different layer numbers; the results for the peak of the Q-NAPP are provided in table 7. The plots of the Q-NAPP are very similar for 1-2-4 layers, but in the case of 8 layers, it shows a significantly lower peak (see Fig.20)

In table 7 the data of the compliance distances and power reduction factor, calculated with the same parameters of section VI are provided. In Fig.21 it is possible to find the plot of the boundary of the exclusion zone for the case $L = 1$. It is worth underlining that the shape and size of the exclusion zone is very different with respect to the one depicted in Fig.6.

The calculation of the NAPP has been repeated for other procedurally generated cities, obtaining again results very similar to the ones in Fig.14; this behavior confirms the validity of the simplified approach used in Section IV, that could be profitably used in the product compliance phase [8]. The use of ray-tracing, or similar site-specific simulation tools, could be, instead, particularly beneficial in the product installation compliance [8], in order to validate the achieved compliance boundaries.

As a final consideration, the polarization of the radiating elements does not seem to have a significant impact on the calculation of the NAPP; in some tests performed we have seen that the use of dual polarized elements helps in improv-

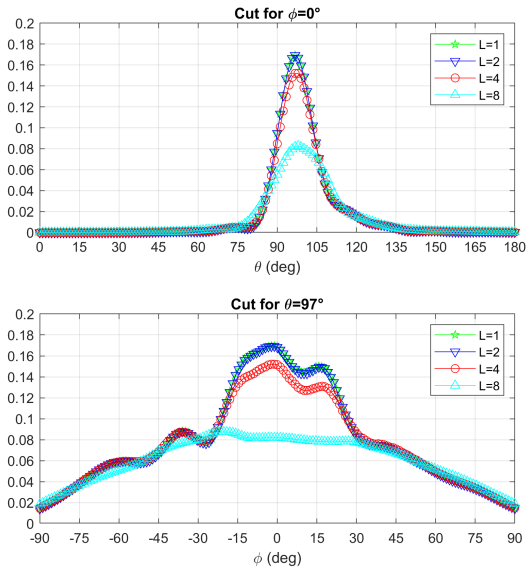

FIGURE 20. Relevant cuts of the Q-NAPP function calculated on 1000 random sets of $K = 200$ random users in the city when multiple layers are employed.

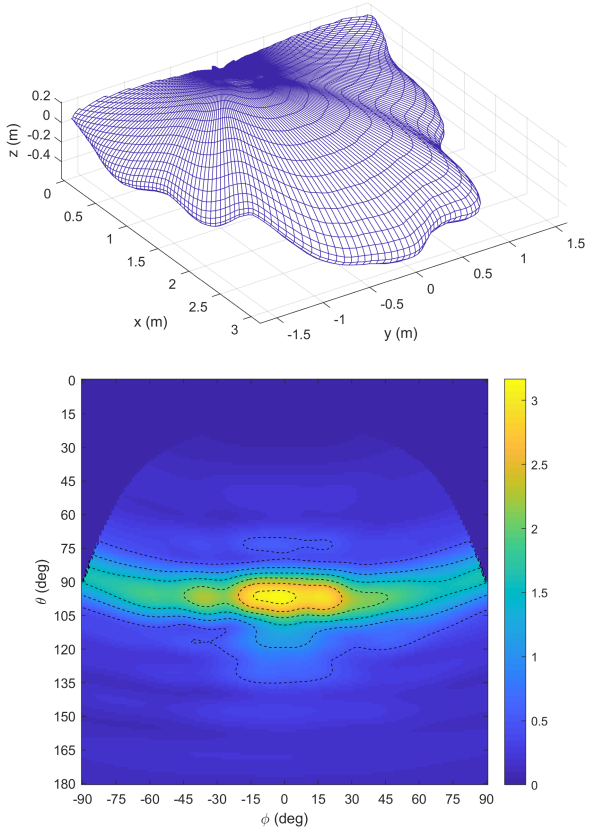

FIGURE 21. The exclusion zone calculated from the 95% quantile of NAPP function calculated on 1000 random sets of $K = 200$ random users in the city with $L = 1$. Upper plot: 3D representation of the boundary of the exclusion zone. Lower plot: imagemap of the $R_{q=0.95}$ function. The contour curves are calculated for the values of the "ticks" of the colorbar.

ing the signal level on the terminals (because of the diversity gain), but does not change significantly the radiated field in the proximity of the BS, that is much more influenced by the number and position of the radiators.

VIII. CONCLUSION

In this paper we have discussed the analysis of the power levels around a 5G antenna array, with the goal to provide a reasonable assessment of the human exposure and the calculation of the compliance boundaries.

In particular, because of the specific nature of the field radiated by a 5G antenna array and its user access method, we have introduced a novel metric for the calculation of the average power density flux around the antenna, the Normalized Average Power Pattern (NAPP).

Such a quantity can be used directly to estimate the average expected power level in a specific point with respect to the peak power level measured when the antenna is focusing its beam in a specific direction, and its quantiles to provide a method to calculate proper bounds for the compliance boundaries around the BS array.

The statistical approach proposed can take into account all the wireless system parameters, and in the paper we have considered an extensive study of the effect of the variation of all the system parameters on the calculation of the NAPP. More specifically:

1) As far as the element pattern is sufficiently "flat" within the coverage area, it plays a minor role on the calculation of the power levels.
2) The number of antennas employed has a strong effect on the NAPP, but also on the antenna gain; the increase of the number of antennas may result in an increase of the size of the compliance region, but this increase is limited.
3) The variation of the extent of the scanning region strongly modifies the NAPP: the wider the region, the smaller the values of the NAPP.
4) The use of grid of beams with a high number of beams provides no significant variations, but the use of grid of beams with few beam introduces some oscillations on the NAPP, but does not change its average behavior.
5) The angular distribution of the users around the array strongly influences the NAPP, and we have noticed a significant difference when the uniformly distributed users on a plane are selected from a triangular cell or from an hexagonal cell.
6) The use of multiple layers communication has a minor impact of the NAPP in the considered cases up to a number of 4 layers; when the layer number is higher, it becomes difficult for the antenna to provide the needed zeros in the direction of the unwanted users and to provide a good directivity in the selected directions, because of the limited number of degrees of freedom of the field radiated by the array in the scanning region [26]. This difficulty results in an average reduction of the antenna gain.

```
function H=QRscheduler(H,L)
% QR scheduler
% H: channel matrix
% L: number of layers
N=size(H,2); % Number of array antennas
P=N/L;       % Number of sets
for k=0:(P-2)
  A=H(:,(1+k*L):end);        % Submatrix extraction
  [~,~,e] = qr(A,'vector'); % Permutation vector e
  H(:,(1+k*L):end)=A(:,e);  % Submatrix sorting
end
```

FIGURE 22. Example code for the QR scheduler.

Most of the presented results have been obtained with a simplified antenna and propagation model; to validate the proposed results we have also considered the case of an array employing dual polarized antenna elements and the users have been placed inside a virtual city, that has been simulated by means of a custom ray tracing model. The obtained results are very similar to the corresponding results calculated by means of the simplified approach, and confirm the effectiveness of the proposed method. As an additional result, we have demonstrated that any model used for the exposure assessment should take into account the aforementioned items, and in particular points 3), 5) and 6) when using more than 4 layers, the angular distribution of users around the BS being apparently the most important.

As a future development we aim to extend the proposed analysis to indoor scenarios, and we plan to exploit the analysis performed to achieve the synthesis of more efficient antenna arrays for 5G applications.

APPENDIX
THE SCHEDULING ALGORITHM

Let us now consider the channel matrix $\mathbf{H} = [\mathbf{h}_1, \ldots, \mathbf{h}_K]$ belonging to the set of complex matrices of dimensions $N \times K$, where K is the number of users, and N is the number of radiating elements. Each column vector $\mathbf{h}_k$ contains the excitations of the N radiating elements when the antenna is focused towards the $k-$th user; just as an example, in the case of free space propagation and a position of the $k-$th users described by (θ_k, ϕ_k), we would have

$$\mathbf{h}_k = e^{j\beta(\mathbf{x}\cos\phi_k \sin\theta_k + \mathbf{y}\sin\phi_k \sin\theta_k + \mathbf{z}\cos\theta_k)} \tag{8}$$

where β is the free-space wavenumber, and $\mathbf{x}$, $\mathbf{y}$ and $\mathbf{z}$ are N length vectors containing the coordinates of the radiating elements of the considered array.

In section V we analysed the use of multiple layers for communication, so we need to group users in sets of $L = 2$, $L = 4$ or $L = 8$ in order to obtain uniform groups, so that we can form $P = K/L$ submatrices $\mathbf{H_p}$ of dimension $N \times L$, so that these submatrices are suitable for the use of the multiplexing approach chosen (in our case the Zero-Forcing method).

If we just perform a partition of the starting $\mathbf{H}$ matrix into submatrices, many of them would not be full rank, and the zero forcing approach could not be fruitfully applied [23].

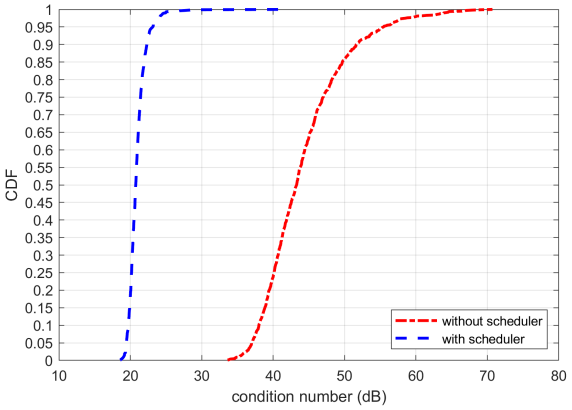

FIGURE 23. Cumulative density function of the distribution of the condition number of the 1000 random 64 × 64 complex matrices.

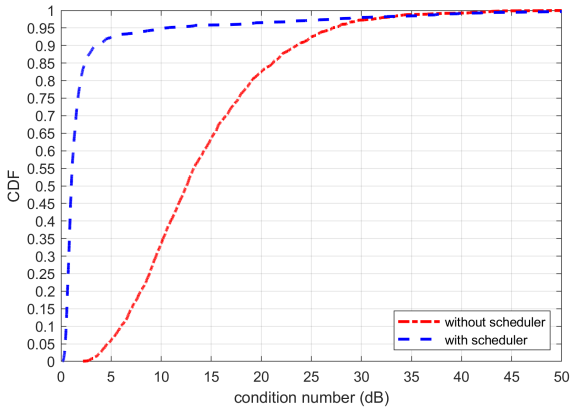

FIGURE 24. Cumulative density function of the distribution of the condition number of the 25 64 × 8 sub-matrices obtained from the 64 × 200 channel matrix.

For this reason we need to perform an ''user scheduling'', a fundamental process for the correct network management, and in 5G communications it becomes even more important.

There are several sub-optimal approaches to this problem that have been proposed in the open literature [27]–[32] (the exhaustive search is the only known method that provides the optimal result but with a overwhelming computational burden). Unfortunately none of the existing algorithms adequately fits our problem; for this reason, we developed a novel scheduling algorithm, based on QR decomposition with column pivoting that differs from ordinary Gram-Schmidt algorithm since it takes the largest remaining column at the beginning of each new step, generating a permutation vector [33]. The permutation vector obtained is the key to obtain the sets: in the first step the QR with pivoting of the channel matrix is computed, and the matrix is sorted according to the QR permutation vector; in the successive $k-$th step the QR calculation is repeated for the sub-matrix obtained excluding the first kL columns of $\mathbf{H}$. An example code in Matlab is provided in Fig.22.

The performances of the QR scheduler are pretty good; to test the algorithm with a very hard problem, in Fig.23 we compare the condition number distribution of 1000 random 64×64 complex matrices, with respect to the condition number of matrices obtained applying the QR scheduler to the 64×64000 matrix with $L = 64$: apart from the matrices generated in the last steps of the scheduling algorithm, the other matrices are full rank with a very good condition number. With reference to the cases considered in the paper, in Fig.24 we show the distribution of the condition number obtainable considering the scanning region of $30° \times 120°$, $K = 200$ and $L = 8$; using the proposed scheduler 95% of the obtained sub-matrices show a condition number smaller than 10dB, making this approach suitable for zero-forcing beamforming. The calculation of the scheduling is also pretty quick, since in the $K = 200$ / $L = 8$ case it requires less than 30ms using Matlab and an Intel Core i7 8700K CPU.

REFERENCES

[1] *Radio Transmission and Reception (Release 15), 3GPP Technical Specification Group Radio Access Network; NR*, document TS 38.104, v15.5.0, May 2019.

[2] D. Tse and P. Viswanath, *Fundamentals of Wireless Communication*. Cambridge, U.K.: Cambridge Univ. Press, 2005.

[3] E. G. Larsson, O. Edfors, F. Tufvesson, and T. L. Marzetta, ''Massive MIMO for next generation wireless systems,'' *IEEE Commun. Mag.*, vol. 52, no. 2, pp. 186–195, Feb. 2014.

[4] S. Persia, C. Carciofi, S. D'Elia, and R. Suman, ''EMF evaluations for future networks based on massive MIMO,'' in *Proc. IEEE 29th Annu. Int. Symp. Pers., Indoor Mobile Radio Commun. (PIMRC)*, Sep. 2018, pp. 1197–1202.

[5] M. D. Migliore, ''Horse (electromagnetics) is more important than horseman (information) for wireless transmission,'' *IEEE Trans. Antennas Propag.*, vol. 67, no. 4, pp. 2046–2055, Apr. 2019.

[6] A. Ahlbom, U. Bergqvist, J. H. Bernhardt, J. P. Cesarini, M. Grandolfo, M. Hietanen, A. F. Mckinlay, M. H. Repacholi, D. H. Sliney, J. A. Stolwijk, and M. L. Swicord, ''Guidelines for limiting exposure to time-varying electric, magnetic, and electromagnetic fields (up to 300 GHz),'' *Health Phys.*, vol. 74, no. 4, pp. 494–521, 1998.

[7] International Commission on Non-Ionizing Radiation Protection, ''Guidelines for limiting exposure to electromagnetic fields (100 kHz to 300 GHz),'' *Health Phys.*, vol. 118, no. 5, pp. 483–524, May 2020.

[8] *Determination of RF Field Strength, Power Density and SAR in the Vicinity of Radiocommunication Base Stations for the Purpose of Evaluating Human Exposure*, IEC Standard 62232, 2017.

[9] S. Adda, T. Aureli, S. D'Elia, D. Franci, E. Grillo, M. D. Migliore, S. Pavoncello, F. Schettino, and R. Suman, ''A theoretical and experimental investigation on the measurement of the electromagnetic field level radiated by 5G base stations,'' *IEEE Access*, vol. 8, pp. 101448–101463, 2020.

[10] R. Pawlak, P. Krawiec, and J. Zurek, ''On measuring electromagnetic fields in 5G technology,'' *IEEE Access*, vol. 7, pp. 29826–29835, 2019.

[11] S. Aerts, L. Verloock, M. Van Den Bossche, D. Colombi, L. Martens, C. Tornevik, and W. Joseph, ''*In-situ* measurement methodology for the assessment of 5G NR massive MIMO base station exposure at sub-6 GHz frequencies,'' *IEEE Access*, vol. 7, pp. 184658–184667, 2019.

[12] H. Keller, ''On the assessment of human exposure to electromagnetic fields transmitted by 5G NR base stations,'' *Health Phys.*, vol. 117, no. 5, pp. 541–545, Nov. 2019.

[13] D. Franci, S. Coltellacci, E. Grillo, S. Pavoncello, T. Aureli, R. Cintoli, and M. D. Migliore, ''Experimental procedure for fifth generation (5G) electromagnetic field (EMF) measurement and maximum power extrapolation for human exposure assessment,'' *Environments*, vol. 7, no. 3, p. 22, Mar. 2020.

[14] D. Franci, S. Coltellacci, E. Grillo, S. Pavoncello, T. Aureli, R. Cintoli, and M. D. Migliore, "An experimental investigation on the impact of duplexing and beamforming techniques in field measurements of 5G signals," *Electronics*, vol. 9, no. 2, p. 223, Jan. 2020.
[15] *IEC TR 62669 ed2 106/463/cd, Case Studies Supporting*, Internation Electromechanical Commission, IEC Standard 62232, Sep. 7, 2018.
[16] B. Thors, A. Furuskar, D. Colombi, and C. Tornevik, "Time-averaged realistic maximum power levels for the assessment of radio frequency exposure for 5G radio base stations using massive MIMO," *IEEE Access*, vol. 5, pp. 19711–19719, 2017.
[17] P. Baracca, A. Weber, T. Wild, and C. Grangeat, "A statistical approach for RF exposure compliance boundary assessment in massive MIMO systems," in *Proc. 22nd Int. ITG Workshop Smart Antennas (WSA)*, 2018, pp. 1–6.
[18] D. Colombi, P. Joshi, R. Pereira, D. Thomas, D. Shleifman, B. Tootoonchi, B. Xu, and C. Tornevik, "Assessment of actual maximum RF EMF exposure from radio base stations with massive MIMO antennas," in *Proc. Photon. Electromagn. Res. Symp. Spring (PIERS-Spring)*, Jun. 2019, pp. 570–577.
[19] R. Werner, P. Knipe, and S. Iskra, "A comparison between measured and computed assessments of the RF exposure compliance boundary of an *in-situ* radio base station massive MIMO antenna," *IEEE Access*, vol. 7, pp. 170682–170689, 2019.
[20] D. Colombi, P. Joshi, B. Xu, F. Ghasemifard, V. Narasaraju, and C. Törnevik, "Analysis of the actual power and EMF exposure from base stations in a commercial 5G network," *Appl. Sci.*, vol. 10, no. 15, p. 5280, Jul. 2020.
[21] M. D. Migliore, "On electromagnetics and information theory," *IEEE Trans. Antennas Propag.*, vol. 56, no. 10, pp. 3188–3200, Oct. 2008.
[22] M. D. Migliore, "An intuitive electromagnetic approach to MIMO communication systems [wireless corner]," *IEEE Antennas Propag. Mag.*, vol. 48, no. 3, pp. 128–137, Jun. 2006.
[23] H. Yang and T. L. Marzetta, "Performance of conjugate and zero-forcing beamforming in large-scale antenna systems," *IEEE J. Sel. Areas Commun.*, vol. 31, no. 2, pp. 172–179, Feb. 2013.
[24] E. Bjornson, L. Sanguinetti, J. Hoydis, and M. Debbah, "Optimal design of energy-efficient multi-user MIMO systems: Is massive MIMO the answer?" *IEEE Trans. Wireless Commun.*, vol. 14, no. 6, pp. 3059–3075, Jun. 2015.
[25] H. L. Bertoni, *Radio Propagation for Modern Wireless Systems*. London, U.K.: Pearson, 1999.
[26] M. D. Migliore, "On the role of the number of degrees of freedom of the field in MIMO channels," *IEEE Trans. Antennas Propag.*, vol. 54, no. 2, pp. 620–628, Feb. 2006.
[27] L. Jin, Z. Hu, and X. Gu, "Low-complexity scheduling strategy for wireless multiuser multiple-input multiple-output downlink system," *IET Commun.*, vol. 5, no. 7, pp. 990–995, May 2011.
[28] C. Y. Zhang, M. Q. Wu, R. Q. Chen, and G. D. Ma, "Novel user scheduling schemes based on nonlinear precoding for multiuser MIMO systems," *Appl. Mech. Mater.*, vol. 195, pp. 270–276, Aug. 2012.
[29] T. E. Bogale, L. B. Le, and A. Haghighat, "User scheduling for massive MIMO OFDMA systems with hybrid analog-digital beamforming," in *Proc. IEEE Int. Conf. Commun. (ICC)*, Jun. 2015, pp. 1757–1762.
[30] M. Benmimoune, E. Driouch, W. Ajib, and D. Massicotte, "Joint transmit antenna selection and user scheduling for massive MIMO systems," in *Proc. IEEE Wireless Commun. Netw. Conf. (WCNC)*, Mar. 2015, pp. 381–386.
[31] X. Liu and X. Wang, "Efficient antenna selection and user scheduling in 5G massive MIMO-NOMA system," in *Proc. IEEE 83rd Veh. Technol. Conf. (VTC Spring)*, May 2016, pp. 1–5.
[32] G. Lee and Y. Sung, "MAC layer design for mmWave massive MIMO," in *mmWave Massive MIMO*. Amsterdam, The Netherlands: Elsevier, 2017, pp. 227–255.
[33] G. H. Golub and C. F. Van Loan, *Matrix Computations* (Johns Hopkins Studies in the Mathematical Sciences). Baltimore, MD, USA: Johns Hopkins Univ. Press, 1996. [Online]. Available: https://books.google.it/books?id=mlOa7wPX6OYC

DANIELE PINCHERA (Senior Member, IEEE) received the Dr.Eng. degree (summa cum laude) in telecommunication engineering and the Ph.D. degree in information and electronic engineering from the University of Cassino and Southern Lazio, Cassino, Italy, in 2004 and 2008, respectively. He is currently a Tenured Researcher with the Department of Electrical and Information Engineering (DIEI), University of Cassino and Southern Lazio. He is also a member of ELEDIA@UniCAS. His current research interests include smart antennas and multiple-input-multiple-output systems, special purpose antennas, large array synthesis, radar systems, satellite communications, compressed sensing, sensor networks, and industrial and medical applications of microwaves. He is a member of the Italian Electromagnetic Society (SIEm) and the National Interuniversity Consortium for Telecommunication (CNIT). He serves as a Referee of many scientific journals, including the IEEE TRANSACTIONS ON ANTENNAS AND PROPAGATION and the IEEE ANTENNAS AND WIRELESS PROPAGATION LETTERS. He is also an Editor of *Wireless Communications and Mobile Computing*.

MARCO MIGLIORE (Senior Member, IEEE) received the Laurea degree (Hons.) and the Ph.D. degree in electronic engineering from the University of Naples, Naples, Italy. He was a Visiting Professor with the University of California at San Diego, La Jolla, CA, USA, in 2007, 2008, and 2017, the University of Rennes I, Rennes, France, in 2014 and 2016, the Centria Research Center, Ylivienka, Finland, in 2017, the University of Brasilia, Brasil, in 2018, and Harbin Technical University, China, in 2019. He is currently a Full Professor with the University of Cassino and Southern Lazio, Cassino, Italy, where he is also the Head of the Microwave Laboratory and the Director of studies of the ITC courses. He is a member of the ELEDIA@UniCAS Research Laboratory,(National Interuniversity Research Center on the Interactions between Electromagnetic Fields and Biosystems (ICEMmB), where he is the Leader of the 5G Group, Italian Electromagnetic Society (SIEM) and the National Interuniversity Consortium for Telecommunication (CNIT). His current research interests include connections between electromagnetism and information theory, analysis, synthesis, and characterization of antennas in complex environments, antennas and propagation for 5G, ad hoc wireless networks, compressed sensing as applied to electromagnetic problems, and energetic applications of microwaves. He was a Speaker at the Summer Research Lecture Series of the UCSD CALIT2 Advanced Network Science, in 2008. He serves as a referee for many scientific journals. He has served as an Associate Editor for the IEEE TRANSACTIONS ON ANTENNAS AND PROPAGATION.

FULVIO SCHETTINO (Member, IEEE) received the Laurea degree (Hons.) and the Ph.D. degree in electronic engineering from the University of Naples, Naples, Italy. He is currently an Associate Professor with the University of Cassino and Southern Lazio, Cassino, Italy. He is a member of the ELEDIA@UniCAS Research Laboratory, National Interuniversity Research Center on the Interactions between Electromagnetic Fields and Biosystems (ICEMmB), the Italian Electromagnetic Society (SIEM) and the National Interuniversity Consortium for Telecommunication (CNIT). His current research interests include numerical electromagnetics, regularization methods, the connections between electromagnetism and information theory, the analysis, synthesis and characterization of antennas in complex environments, antennas and propagation for 5G, and energetic applications of microwaves.